IEEE Robotics and Automation Letters (RAL) paper presented at the
2020 IEEE/RSJ International Conference on Intelligent Robots and Systems (IROS)
October 25-29, 2020, Las Vegas, NV, USA (Virtual)

Stable Autonomous Spiral Stair Climbing of Tracked Vehicles using Wall Reaction Force

Shotaro Kojima[1,2], Kazunori Ohno[3,4], Takahiro Suzuki[3],
Yoshito Okada[4,2], Thomas Westfechtel[3], and Satoshi Tadokoro[2]

***Abstract*— In this paper, an autonomous spiral stair climbing method for tracked vehicles using the reaction force from side walls has been proposed. Spiral stairs are one of the most difficult terrains for tracked vehicles because of their asymmetrical ground shape and small turning radius. Tracked vehicles are expected to be used in industrial plant inspection tasks, where robots should navigate on multiple floors by ascending the stairs. Spiral or curved stairs are installed as part of inspection passages for cylindrical facilities, such as boilers, chimneys, or large tanks. Previously, the authors have experimentally demonstrated that the wall-following motion is effective for stabilizing and accelerating spiral stair climbing. However, the complete automation of climbing motion or the analysis of why the same motion is generated even if a disturbance exists in the initial entry angle to the wall should be investigated. In this study, the authors developed an autonomous spiral stair climbing method using the wall reaction force and clarified the applicable limitations of this method using a geometrical model. Autonomous spiral stair climbing is realized by attaching passive wheels on its collision point and automating the motions of main tracks and sub-tracks. The geometrical model shows the expected trajectory of the robot on the spiral stairs, which suggests that the robot' s rotation radius converges to a specific value; this is experimentally confirmed by measuring the robot's motion. The wall-following motion of robots is equivalent to human inspectors grasping handrails while climbing stairs. Through collisions with surrounding objects, motion is stabilized and certainty is guaranteed.**

I. Introduction

Tracked vehicles are expected to be used in industrial plant inspection tasks, where robots should navigate on multiple floors by ascending stairs. Spiral or curved stairs are installed as part of inspection passages for tall cylindrical facilities, such as boilers, chimneys, or large tanks. In such a case, the staircase is attached to the cylindrical surface to inspect the facility as closely as possible. In other cases, spiral stairs are installed only for reducing space because of the smaller footprint of the staircase than that of straight stairs.

Spiral stairs are one of the most difficult terrains for tracked vehicles because of their asymmetrical ground shape and small turning radius. Although the robot must rotate to the inner side of the staircase when it is climbing up, this is nearly impossible because of the asymmetrical ground shape, which causes one of the left or right tracks to slip during rotational motion. The asymmetrical ground shape causes the slippage of the left or right track when the robot rotates on the spiral stairs, which complicates its rotation on the terrain.

Previously, the authors experimentally demonstrated that the wall-following motion was effective for stabilizing and accelerating spiral stair climbing motion [1]. A side wall is often attached to the handrail to prevent tools or components from collapsing. A robot follows the wall with its passive wheels attached to the side surface of the sub-tracks, as shown in Fig.1-(a). Rotational motion is generated using the geometrical constraint of the wall. In our previous study, we demonstrated the improved performance of a manual operation in terms of speed using a wall-following motion on spiral stairs. In addition, we experimentally demonstrated that the method is available in several initial states with different entry angles to the wall. The wall-following motion of robots is similar to human inspectors grasping handrails during stair climbing. Through collisions with surrounding objects, motion is stabilized and certainty is guaranteed. However, the complete automation of the climbing motion requires further investigation. To fully automate spiral stair climbing, the motion of the main-tracks and sub-tracks should be autonomously controlled. In spiral stairs, it is difficult to accurately detect the position of a robot because of slippage on the stairs. Hence, sensor-reflective motion control was used in the proposed method. When deciding the sub-track's motion, the controller should consider that the sub-tracks do not kick the stairs, and that the robot must obtain sufficient

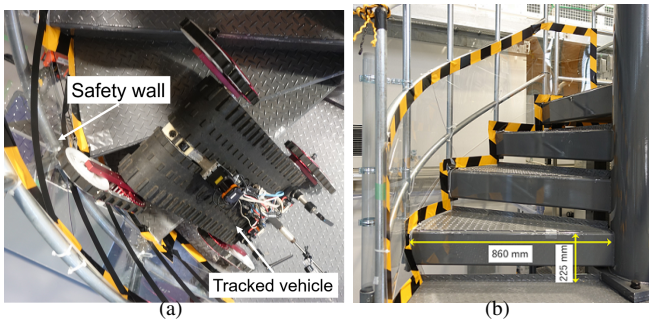

Fig. 1. (a) Tracked vehicle "Quince" climbing up spiral stairs using reaction force from safety wall and (b) target spiral staircase with safety wall.

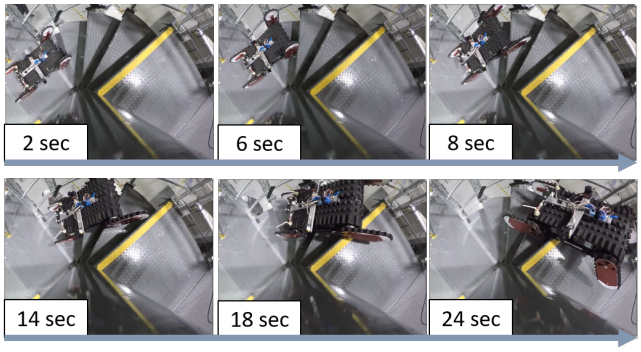

Fig. 2. Snapshot of autonomous spiral stair climbing. This is realized by constructing motion control method which actively utilize collision force for the rotational motion.

[1]Author is a JSPS Research Fellow.
[2]Authors are with the Graduate School of Information Sciences, Tohoku University, Sendai, Japan.
[3]Authors are with NICHe Tohoku University, Sendai, Japan.
[4]Authors are with RIKEN Center for AIP.
Shotaro Kojima: kojima@rm.is.tohoku.ac.jp

rotational moment from the collision force on the side surface of the sub-tracks. The main-track motion should be decided by considering the trade-off between obtaining the collision force and minimizing slippage. Slippage is a major reason for failure in spiral stair climbing. Hence, the sub-tracks and main-tracks should be controlled to minimize slippage. In this paper, the authors construct an autonomous spiral stair climbing method using reaction force from the wall as shown in Fig.2 and clarify the applicable limitations of this method using a geometrical model. Main-track's motion is experimentally derived to minimize the slippage and keep collision to the wall. Sub-track's motion is controlled to keep flat on the stair, which prevents falling down and obtaining rotational moment by collision force from the wall. A geometrical model is used for analysis and it shows that the robot's trajectory converges to a specific radius though the initial entry angle is different, because of the geometrical constraint of the wall. Main contributions of this paper are as follows:

- An autonomous spiral stair climbing method that generates a series of motions, enters the stairs, climbs up, and reaches the upper floor is proposed.
- A two-dimensional LiDAR-based sensor reflective approach is used to determine two main-tracks and four sub-track motions. These motions are generated to obtain sufficient rotational moment from wall reaction force and to keep main-tracks catching the ground.
- The proposed method enables a robot to automatically climb spiral stairs with a 100% success rate.
- Geometrical analysis shows that a passive convergence mechanism exists, in which the robot trajectory converges to a specific radius during wall-following motion, even when the initial entry angle to the wall is changed.

II. Related Work

Investigations regarding stair-climbing motion is being actively conducted because search and rescue robots are expected to be used on rough terrains.

Several methods have been proposed for automating stair climbing using a sensor-reflective approach [2], [3], [4], [5], [6], [7], which involve autonomous sub-track control that employ sensors on the robot. Our proposed method is related to these approach and control sub-tracks based on LiDAR sensor data. In spiral stair climbing, the tracked vehicle must rotate while climbing up the stairs. Our proposed method realizes rotational motion on the stairs using the reaction force from the side walls. Hence, we must consider not only preventing the robot from falling down, but also the method to obtain the collision force when designing the motion.

Another approach, which is a planning-based approach for autonomous stair climbing, was proposed in [8]. Compared with the sensor-reflective approaches, planning based approach has an advantage that the motion of the robot can be decided before traversing the terrain. In the spiral stairs with a small rotation radius, it is difficult to accurately estimate the position of the robot because of the slippage of tracks. Also, based on our previous studies [9] [1], we estimated that it is difficult to follow the planned path without colliding with the wall in our target environment. Hence, we selected sensor-reflective motion control which actively utilizes the wall reaction force for the rotational motion.

The effectiveness of using contact with the environment, such as walls or obstacles, has been reported for humanoid robots. Several studies have been conducted to overcome rough terrains using contact with walls or handrails for humanoid robots [10], [11], [12]. These approaches are similar to human behaviors for stabilizing postures on rough terrains by grasping or touching surrounding objects. In this study, the wall-following motion is utilized in tracked vehicles to generate rotational motions and stabilize postures.

Research has been conducted regarding the turning motion for generating rotational motions on rough terrains using external forces. David et al. proposed the turning motion on sandy soils for tracked vehicles that use plows [13]. This method enables a rotational motion on sandy ground by fixing the rotational center using a plow. This method is the same as our proposed method in that the turning motion is generated by fixing the rotational center using geometrical constraints.

III. Autonomous spiral stair climbing using wall reaction force

A. Outline

The sensor reflective approach is used for climbing spiral stairs because it can realize a stable motion generation even in a severe environment where slippages occur in the main-tracks or sub-tracks [6][7]. Fig.1-(a) shows our target tracked vehicle, which has six degrees of freedom (DoF) (two main tracks and four subtracks). The six DoF motions were autonomously determined using the sensor-reflective approach. A two-dimensional (2D) LiDAR sensor was used to measure the spiral stair shape. An internal measurement unit (IMU) sensor was used to measure the pose of the main body. Four encoder sensors were used to measure the sub-track angle, and six DoF motions were autonomously determined from these sensor data in real time.

To climb the spiral stairs, a force that moves forward while turning must be generated. The angles of the sub-tracks and velocity of the main-track are determined to generate a large rotational moment, forward motions, and low slippages. The reaction force from the wall was used to generate the rotational moment. When the reaction force is large, a large rotational moment is generated. In addition, when the contact point is located far from the center of the robot's body, it generates a large rotational moment. The main-track motions and sub-track angles should be determined to maximize the rotational moment. However, a large main track motion causes slippage. Trade-offs exist between the larger rotational moment and slippage for the main-tracks. Hence, a good balance between the left and right main track motions must be achieved.

In this section, we describe the control rules of the main-tracks that generate rotational motions and minimize slippage. Furthermore, we describe the control rules of the sub-tracks that prevent the inclination of the main body and reduce slippages. For a full automation in climbing the spiral stairs, not only climbing, but also entering and reaching are required, as shown in Fig.3. In the phase of "Entering" and "Reaching", a sub-track control method in [7] is used, because the requirement for the motion is the same as that in the straight stairs. In "Climbing" phase, We need to consider not only keeping the posture but also how to obtain rotational moment using the wall reaction force. Hence, the detailed discussion of the motion in "Climbing" phase is described in section III-C.

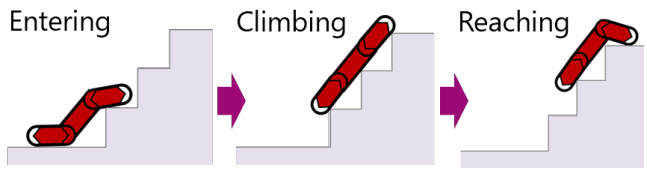

Fig. 3. Motion strategy of sub-tracks during climbing up the stair. First, main body is lifted on the stair using front side flippers. Second, sub-tracks are fully extended during climbing up the stair. Finally, front side sub-tracks are lowered to keep contact to the ground when the robot reach the upper floor.

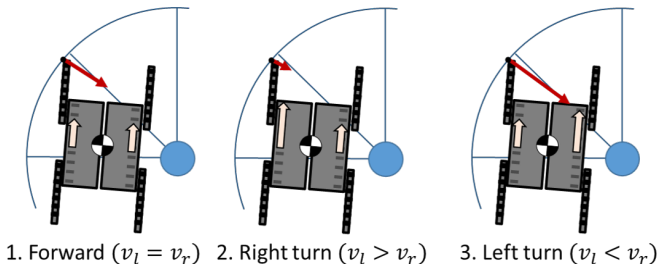

Fig. 4. Relationship between main-track's motion and wall reaction force. The robot can climb up the spiral stair if motion is commanded as pattern 1 or 3. In pattern 2, the robot couldn't climb up because it couldn't obtain sufficient wall reaction force for rotation. Hence, more detailed verification is conducted for pattern 1 and 3.

B. Motion of main-tracks

Here, the movement of the main-track is described for a clockwise climbing spiral staircase. The method described herein is also applicable to counter-clockwise climbing spiral stairs. The tracked vehicle can control the forwarding and turning motions by adjusting the left and right velocities of the main tracks. When the robot climbs up the clockwise spiral stair, it should generate a forward motion and a right turn motion. Using the wall reaction force, the rotational movement in the right direction can be increased.

To determine the operation of the main tracks, the authors tested three conditions of the motion command as shown in Fig.4: 1. The same velocity for the left and right tracks (forward); 2. the velocities of both side tracks are in the same direction, but the left side track is larger (right turn left turn under the conditions of); 3. the velocities of both side tracks are in the same direction, but the right side track is larger (left turn under the conditions of). The test was conducted on the spiral stairs. Consequently, in condition 2 (under the condition of right turn), the robot could not climb the spiral stairs. This is because a significant slippage occurred during turning motion on the stairs. The wall reaction force was not sufficient for the rotational motion, and main-tracks could not generate the forward driving force under the condition. On the other hand, the conditions of forward and left turns like in 1 and 3, which yielded the wall reaction force introduced in a previous study [1], the robot could climb up the stair using the wall reaction force. Hence, we investigated them again under different conditions.

For a more detailed verification, we analyzed several main track motions (one forward motion and two left-turning motions) that are suitable for traversing spiral stairs. The forward motion was evaluated using combination A: ($v_l = 0.10$[m/s], $v_r = 0.10$[m/s]). Left turning motions were evaluated by two combinations, i.e., B: ($v_l = 0.10$[m/s], $v_r = 0.14$[m/s]) and C: ($v_l = 0.10$[m/s], $v_r = 0.16$[m/s]), which changed the magnitude of the wall reaction force. A motion capture system was used to measure the tracked vehicle motion. The moving distance and slippage were calculated from the motion capture data. All these conditions indicate that the collision is maintained during the motion, and that the robot can rotate itself using the reaction force from the wall when it is climbing up the stairs. A constant velocity was imposed for 6.5 seconds for each condition. During the experiment, slippage was identified if the slip amount was larger than 25% of the grouser's interval. The number of slips and the slip distance were counted when slippage was detected.

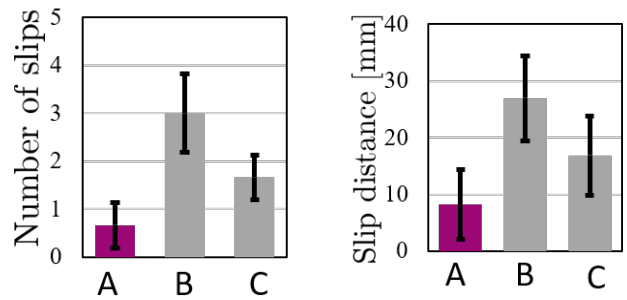

(a) Number of slips (b) Slip distance

Fig. 5. Comparison of slip for each command. The sets of both side track velocities (vl, vr) are as follows: A: (0.10[m/s], 0.10[m/s]), B: (0.10[m/s], 0.14[m/s]), and C: (0.10[m/s], 0.16[m/s]). Slippage is minimized when the same velocity is imposed to both side tracks under condition A.

The results are shown in Fig. 5. At all the conditions, the tracked vehicle could climb up the spiral stairs. However, the difference in slippages was observed depending on the conditions. As shown, the number of slips and the slip distance were minimized when the same velocity was imposed to both side tracks, as in condition A. The results show that condition A (same track velocity) minimizes the slippage because the state where the grousers are trapped on the surface of the stairs can be maintained. Under conditions B and C, the difference between the left and right-side track velocities increased the slippage. The authors assumed that this was caused by the phase difference of the grousers on the left and right tracks. Based on the comparison results, the straightforward motion was discovered to be suitable for the main tracks to minimize slippages during collision.

Based on the results, we set the same velocity for the left and right main-tracks to use the wall reaction force to climb up the spiral stairs.

C. Motion of sub-tracks

Motion of sub-tracks in "Climbing" phase in Fig.3 is discussed considering how to keep the robot's posture and how to obtain rotational moment using the wall reaction force. Here, the flipper control in "Climbing" phase is discussed from the perspective of 1) obtaining rotational moment and 2) preventing catches with the wall or the ground.

1) Obtaining rotational moment: Fig.6 shows rotational moment obtained from the wall reaction force. This figure considers three cases: (a)sub-tracks are kept flat, (b) sub-tracks are lowered, and (c) sub-tracks are raised. The distance between the collision point and the robot's center is maximized in (a), so that the largest rotational moment is obtained if the wall reaction force is the same. Thus, (a) keeping sub-tracks flat is the best choice in terms of rotational moment by wall reaction force.

2) Preventing catches with the wall or the ground: Fig. 7 shows the possible reasons for catches with the wall or

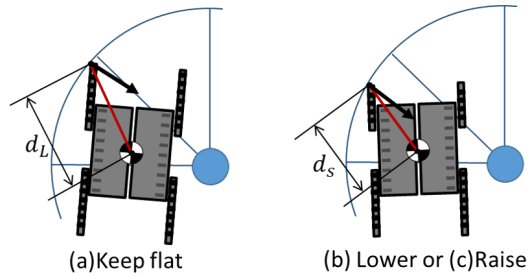

Fig. 6. Rotational moment obtained from the wall reaction force in three cases: (a)front sub-tracks are kept flat, (b)front sub-tracks are lowered, and (c)front sub-tracks are raised. the distance between the collision point and the robot's center is maximized in (a), so that the largest rotational moment is obtained if the wall reaction force is the same.

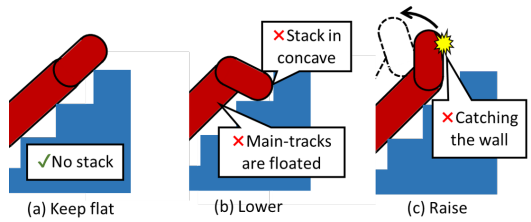

Fig. 7. Possible reasons for catches with the wall or the ground. There is no catch if sub-tracks are kept flat as (a). The robot is get stacked with the ground if sub-tracks are lowered as (b) and that makes main-tracks floated. If sub-tracks are raised as (c), it catches the wall and causes falling.

the ground. There is no catch if sub-tracks are kept flat as (a). The robot gets stacked with the ground if sub-tracks are lowered as (b) and that makes main-tracks floated, which is also an unsuitable situation for main-track's control because the main-tracks cannot generate forward driving force to climb up the stair. If sub-tracks are raised as (c), sub-tracks catch the wall and the robot starts climbing the wall,that causes falling on the stair. The tracked surface of the sub-track temporally collides the wall in (a) and (c). However, in (c), the collision point is higher than that of (a) and a moment in pitch angle is generated, which causes pitching-over failure. In (a), pitching-over failure is not observed throughout the experiment in section V and VI. Thus, (a) keeping sub-tracks flat is the best choice in terms of prevention of catches with the wall or the ground.

Considering the above two perspectives, sub-tracks should be kept flat during spiral stair climbing.

D. Control strategy for climbing up spiral stairs

Based on section III-B and section III-C, we propose a motion control method on the spiral stair. Based on the results of section III-B, straight-forwarding motion is commanded to main-tracks. Same velocity is commanded to left and right main-tracks during climbing up the stairs. In the experiment in section V and section VI, commanded velocity was 0.10[m/s].

Fig. 8 shows our proposed control algorithm for sub-tracks. This algorithm switches control rules depending on motion phases in Fig.3 by changing the angle limitations depending on the phase. When the robot enters the stair or reaches the next floor, sub-track angles are not limited and the control algorithm works as same as [7], because the wall reaction force is not needed in these phases. In this mode, the sub-tracks are controlled to keep contact to the ground and keep the robot's posture using ground shape information measured by the LIDAR sensor and robot's inclination measured by the IMU sensor. When the robot is climbing up the stair, sub-track angle limitation works and

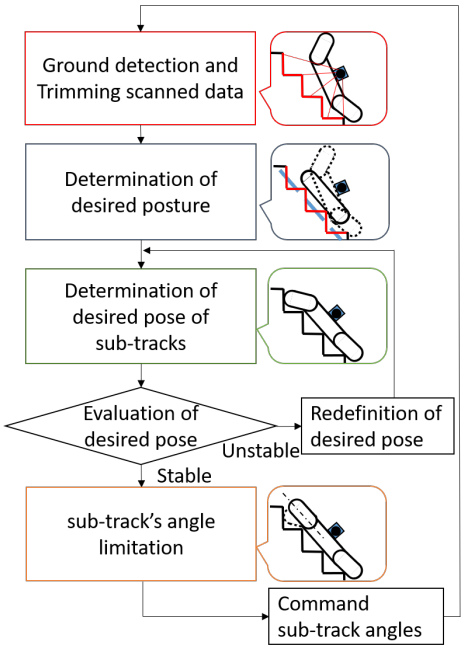

Fig. 8. Algorithm for autonomous sub-track control. The main part is the same as [7]. The angle limitation of the sub-track is introduced during "Climbing" state in Fig.3, to prevent pushing the stair risers.

all the sub-tracks are kept flat, considering the discussions in section III-C.

To detect the "Climbing" phase and switch the control mode, two indicators are used. The first one is the main body's pitch inclination measured by the IMU sensor, whereas the second is the ground detection near the front sub-tracks using LIDAR. The "Climbing" state is detected when the pitch inclination is higher than a threshold, and the ground is detected on the front side of the robot. At the experiment in section V and section VI, the threshold is set to 30°, which is smaller than the stair's inclination. In the "Entering" phase, the robot starts to incline when its front sub-tracks were in the first step. When the inclination exceeded the threshold, the phase is changed to "Climbing," and the control rule is switched. The control rule is reversed when the robot reached the next floor because the ground was not seen on the front side of the robot by the LIDAR sensor when the robot attains the "Reaching" phase.

IV. Geometrical Modeling of Wall-Following Motion for Motion Estimation

A geometrical model is introduced to clarify the reason for passively generating the rotational motion. In our previous study [1], we experimentally discovered that the robot can rotate on spiral stairs provided that collision is maintained, with several conditions of initial entry angle to the wall. However, a few aspects are yet to be elucidated, e.g., why a robot can follow a wall. Here, the geometrical model shows the mechanism by which the angle between the robot and the wall converges to a specific value, if the robot follows the wall because of the geometrical constraints of the wall. This model is based on the assumption that the robot continues colliding with the wall, which satisfy the conditions for stable spiral stairs climbing motion in [1].

A geometrical model is constructed as shown in Fig. 9 to analyze the rotational motion of the robot on a spiral staircase using the wall reaction force. The parameters are listed in Table I.

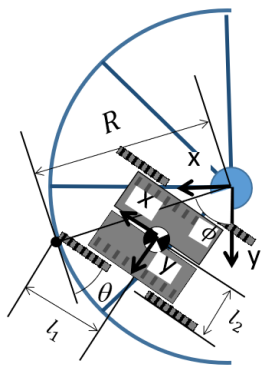

Fig. 9. Geometrical model of tracked vehicles following curved walls

TABLE I
PARAMETERS OF THE GEOMETRICAL MODEL

ϕ	Center angle of the contact point with respect to the staircase center
θ	Angle between the robot body and the wall on contact point
R	Radius of the curved wall
(l_1, l_2)	Relative position of the collision point in the robot coordinate frame
$(v_x^{\text{robot}}, v_y^{\text{robot}})$	Linear velocity of robot in the robot coordinate
$\boldsymbol{R}_{\textbf{robot}}^{\textbf{global}}$	Rotation matrix describing the orientation of the robot local frame with respect to the global frame

In this model, the pose of the robot is uniquely determined by the combination of ϕ and θ because of the constraint where the collision point moves on the wall surface. The global frame is fixed at the center of the spiral staircase. The local frame is fixed on the robot, where the X-axis faces the front and the Y-axis faces the left. The collision point is assumed to move freely on the wall surface because passive wheels are attached on the side surface of the robot to reduce friction.

The position of the robot on the global frame (x, y) is described using θ and ϕ as shown in (1) and (2).

$$x = R\cos\phi - l_1\sin(\theta+\phi) - l_2\cos(\theta+\phi) \quad (1)$$
$$y = R\sin\phi + l_1\sin(\theta+\phi) - l_2\sin(\theta+\phi) \quad (2)$$

(3) is obtained by differentiating (1) and (2) and applying the coordinate frame transformation from the global to the local frame.

$$\begin{bmatrix} \dot{\phi} \\ \dot{\theta} \end{bmatrix} = \frac{1}{R(-l_1\cos\theta + l_2\sin\theta)} \times \begin{bmatrix} l_1 & l_2 \\ R\sin\theta - l_1 & R\cos\theta - l_2 \end{bmatrix} \begin{bmatrix} v_x^{\text{robot}} \\ v_y^{\text{robot}} \end{bmatrix} \quad (3)$$

(3) shows the relationship between the linear velocity of the robot and the angle change on the global frame for a small duration. The detailed derivation process is shown in the Appendix part because the mathematical derivation is not the main contribution of this study.

In this study, the robot trajectory is predicted based on the model. The authors hypothesize that the robot trajectory converges to a curve with a constant radius because of the constraint, which is verifiable based on the model. (3) shows the relationship between the linear velocity of the robot and the angle change on the global frame in a small duration. To simulate the robot trajectory, the velocity of the robot center, $(v_x^{\text{robot}}, v_y^{\text{robot}})$ should be determined to solve (3). Therefore, velocity is determined as a constant forward ($v_x^{\text{robot}} = 0.1$[m/s], $v_y^{\text{robot}} = 0.0$[m/s]), which contains an assumption where the forward velocity is constant and lateral slippage can be ignored.

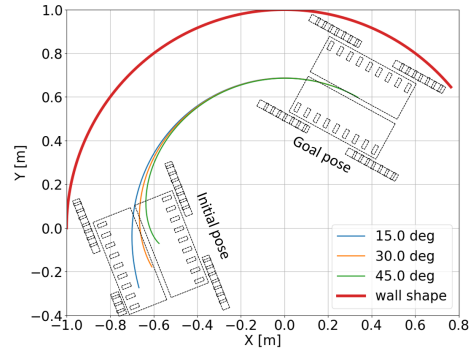

Fig. 10. Robot trajectories predicted from the model for each initial value of θ. All trajectories converge to a curve with a constant radius.

(ϕ, θ) for each time step is derived by sequentially integrating $(\dot{\phi}, \dot{\theta})$ using (3). The robot trajectory is obtained by substituting (θ, ϕ) into (1) and (2). Fig. 10 shows the robot trajectory predicted by the model. As shown, the robot trajectory follows a curve with constant radius. These results indicate that a mechanism exists that enables a constant robot trajectory when the robot follows the wall.

In (3), the term of $R\sin\theta - l_1$, which is a coefficient of v_x in the equation of $\dot{\theta}$ works for convergence of θ because the sign of $\dot{\theta}$ changes when $R\sin\theta - l_1 = 0$. Thus, the value of θ after convergence is described as (4).

$$\theta_{\text{conv}} = \arcsin\left(\frac{l_1}{R}\right) \quad (4)$$

On the other hand, the minimum value of θ, which is achieved when both of the front and rear sub-tracks collide with the wall, is described as (5).

$$\theta_{\min} = \arcsin\left(\frac{l_1}{2R}\right) \quad (5)$$

Comparing (4) and (5), θ_{conv} is larger than $\theta_{\min}$. Thus, after the convergence, θ is larger than $\theta_{\min}$ and rear sub tracks are floated from the wall. (4) is based on a premise of scale where $l_1 < R$, which is satisfied in our target environment and the robot. If this premise is not satisfied, which means that the robot's body size l_1 is relatively large compared with the stair radius R, $\dot{\theta}$ is always negative and θ monotonically decreases before it achieves $\theta_{\min}$.

In terms of maximum value of θ, (6) is given.

$$\theta_{\max} = \arctan\left(\frac{l_1}{l_2}\right) \quad (6)$$

If $\theta > \theta_{\max}$, the sign of denominator of $\dot{\theta}$ $(R(-l_1\cos\theta + l_2\sin\theta))$ is inverted and θ diverges. However, in our target

environment, it was physically impossible to achieve $\theta_{\max}$ because of the narrow passage.

V. Evaluation

We conducted two evaluations in this study. First, the wall following motion was effective for spiral stair climbing using the geometrical model described in Section V-A. Next, the performance of autonomous spiral stair climbing was compared with that of a manual operation. In this experiment, tracked vehicle "Quince" in Fig. 1-(a) is used. The body parameters in Table I are as follows: $l_1 = 0.35[\mathrm{m/s}], l_2 = 0.25[\mathrm{m/s}]$. The weight of the robot is 33kg and it has 10kg payload. The maximum linear velocity is 0.5 [m/s]. Experiments are conducted on the spiral stairs in Fig.1-(b), which has 0.86 [m] radius and 0.23 [m] height steps.

A. verification of trajectory convergence during wall-following motion

In Section VI-A, the trajectory estimation by the model is compared with the actual robot's trajectory, and the convergence of the entry angle θ is shown from the experimental results. Robot trajectories are estimated with the initial entry angle of 30° by measuring the robot pose using a motion capture camera on a spiral staircase. To demonstrate the convergence of the entry angle to the wall, time change of the entry angle θ is measured using the motion capture information and the wall shape. The entry angle is measured under three initial conditions: $\theta = 15°, 30°$, and $45°$, to demonstrate that the angle converges to a specific value that does not depend on the initial state. To confirm that the assumption of ignoring lateral slippage , $v_y^{\mathrm{robot}} = 0$ in (9), longitudinal velocity v_x and lateral velocity v_y is measured using motion capture camera.

B. Autonomous spiral stair climbing

Autonomous spiral stair climbing was performed, as described in Section VI-B. The robot autonomously climbed up the stairs seven times, and the traversal time was measured. During the motion, the pitch inclination of the robot body was measured using a motion capture camera, and the flipper angle was recorded using a rotary encoder inside the robot. To confirm the effect of the angle limitation shown in Fig. 8, which is newly introduced herein, the same experiment was conducted using WITHOUT to record the limitation and sub-track angle. For comparison, the same motion was performed manually by three human operators, in which both main tracks and sub-tracks were manually controlled.

VI. Results

A. verification of trajectory convergence during wall-following motion

Fig. 11 shows the result of the robot trajectory measurement with an initial entry angle of 30°. This figure shows that the predicted trajectory is within the standard deviation of the measured trajectory, indicating that the model successfully predicted the robot's motion.

Fig. 12 shows the time change of the entry angle to the wall θ with three initial conditions: $15°, 30°$, and $45°$. As shown, the angle converged to values between 25° and 30°.

Fig. 13 shows time series data of velocity with 30° initial entry angle. As shown, absolute value of lateral velocity v_y changes near zero, except the moment when longitudinal slip occurred temporally in 5.0 sec, 9.0 sec, 12.5 sec, 17.0 sec, and 19.0 sec.

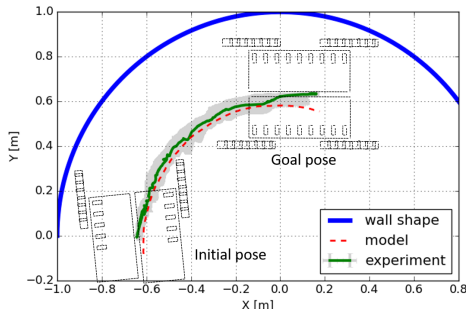

Fig. 11. Comparison of robot trajectories when $\theta = 30°$ for the initial condition. The dashed red line was derived from the model. The solid green line is the mean trajectory for five measurements, and the filled area shows its standard deviation. This result shows that the model can successfully predict the motion of the robot.

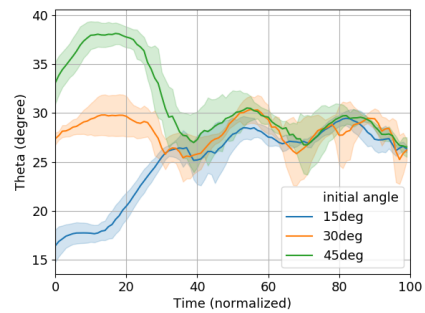

Fig. 12. Time change of entry angle θ with three initial conditions: $15°, 30°$, and $45°$. In all conditions, θ converged to the same value.

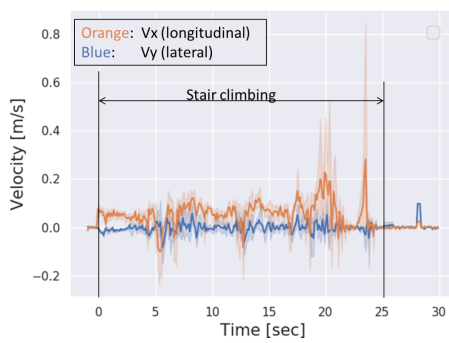

Fig. 13. Time series data of velocity. Initial entry angle is 30°. Orange shows longitudinal velocity v_x^{robot} and blue shows lateral velocity v_y^{robot}. rigid line shows mean value of five trials and shadow area shows standard deviation.

B. Autonomous spiral stair climbing

Fig. 14 shows a snapshot of the autonomous spiral stair climbing. The robot successfully climbed up the stairs for all the trials, and the average operation time was 30.1 s.

Fig.15 shows the pitch inclination during an autonomous climbing trial. As shown in the figure, the maximum inclination angle was 53°.

Fig. 16 shows the time series data of the angle of the front-right sub-track during autonomous spiral stair climbing. The blue line shows the results of our proposed method. The sub-track was raised when the robot entered the stairs, remained flat during climbing, and lowered when it arrived at the upper floor. This result shows that the strategy shown in Fig. 3 was realized. For comparison, the yellow line shows the result of the WITHOUT subtrack angle limitation originally introduced herein. In this case, the robot was stacked on the

stair in all trials because the sub-tracks were lowered on the stairs.

Fig.17 shows a comparison of the operation time. As shown, the operation time of the proposed method was faster than those of operators B and C. The operation time of operator A was slightly more than that of the proposed method.

The results show that the proposed method successfully realized autonomous spiral stair climbing, and that its operation time was faster than those of the two operators in the experiment.

The results show that the proposed method successfully realized autonomous spiral stair climbing, and the performance of operation time is faster than two operators in the experiment.

VII. Discussion

As shown in Section VI-A, the robot trajectories were successfully predicted using the geometrical model shown in Fig. 11. As shown in Fig. 13, absolute value of lateral velocity v_y changes near zero, except the moment when slip occurred temporally in 5.0 sec, 9.0 sec, 12.5 sec, 17.0 sec, and 19.0 sec. At these moments,there is a tendency that lateral and longitudinal slippage occurred at the same time. Based on this result, the authors concluded that the assumption of $v_y = 0[\mathrm{m/s}]$ is suitable with the actual phenomenon because the increase of the lateral slippage was not continuous. Whereas, the results suggest that there is a room for improvement in simulation accuracy by considering temporally slips of tracks. In addition, as shown in Fig. 12, the angle between the robot and the wall converged to a range between $25°$ and $30°$. These results indicate that the geometrical model can describe the robot motion during collision, and the suggestion of the passive-convergence mechanism is confirmed by the results. Whereas, there is a difference in convergence value of θ between expected value of θ_{conv} and actual value. Based on (4), the estimated value of θ_{conv} was $24°$ ($l_1 = 0.35$ [m], $R = 0.86$ [m]), which is slightly smaller than the experimental results ($25°$ - $30°$). The authors assume that this error is caused by the deformation of the wall because the wall was made of polycarbonate plate with 2 mm thickness. θ_{conv} gets larger if the value of stair radius R is smaller, which can be occur if the wall is deformed by the collision force from the robot. Although the accurate estimation of θ_{conv} requires the premise of rigid wall, the model already guarantees the passive convergence mechanism in any radius of staircases, which plays an important role in stable spiral stair climbing.

As shown in Section VI-B, autonomous spiral stair climbing was successfully performed. Fig.17 shows that the operation time of the autonomous operation was more than those of the two human operators. It was assumed that the robot stopped frequently when a motion was commanded to sub-tracks when human operators were employed. Meanwhile, the robot continuously climbed the stairs in the autonomous operation, which is advantageous. Operator A did not stop the robot while controlling the sub-tracks, and he operated the sub-tracks minimally. This resulted in a faster locomotion compared with those of the other two operators, similar to the autonomous operation.

As shown in Fig. 14, the robot can autonomously climb the spiral stairs when the sub-track control algorithm shown in Fig. 8 was applied. The authors introduced a flipper angle limitation to an existing method [7] to realize the strategy described in Section III, which enabled spiral stair climbing. As indicated by the blue line in Fig. 16, the robot can climb the stairs if the angle limitation is introduced. If this limitation is not introduced, as indicated by the yellow line in Fig. 16, the robot always becomes stacked on the stairs. This is because the sub-track control algorithm in [7] commands the sub-track angle to remain in contact with the ground even on the stairs, and the subtracks kick the stair risers, as predicted in Section III-C. Sub-track angle limitations prevented such undesirable motions and enable spiral stair climbing.

VIII. Conclusion

The authors proposed an autonomous spiral stair climbing method for tracked vehicles using the reaction force from the side walls. The autonomous spiral stair climbing method was formulated by automating main tracks and sub-tracks. Using the proposed method, the tracked vehicle automatically climbed up the spiral stairs at a 100% success rate. The operation time was faster than those of two human operator's manual operations. A geometrical model was used to analyze the tracked vehicle's stair climbing motion. The geometrical model showed that a mechanism existed that converged the angle between the tracked vehicle and the wall to a constant value regardless of the initial value. This was experimentally confirmed using a real tracked vehicle and spiral stairs.

Appendix

The derivation process from (1) and (2) to (3) is described in this section. Differentiating both sides of (1) and (2) with respect to time yields the linear velocity, as shown in (7) and (8), respectively.

$$\begin{aligned}\dot{x} &= \{-R\sin\phi - l_1\cos(\theta+\phi) + l_2\sin(\theta+\phi)\}\dot{\phi} \\ &\quad +\{-l_1\cos(\theta+\phi) + l_2\sin(\theta+\phi)\}\dot{\theta} \qquad (7)\\ \dot{y} &= \{-R\cos\phi - l_1\cos(\theta+\phi) + l_2\sin(\theta+\phi)\}\dot{\phi} \\ &\quad +\{-l_1\cos(\theta+\phi) + l_2\sin(\theta+\phi)\}\dot{\theta} \qquad (8)\end{aligned}$$

The orientation of the robot local frame with respect to the global frame is described as a rotation matrix as shown in (9) .

$$\boldsymbol{R}^{\mathbf{global}}_{\mathbf{robot}} = \begin{bmatrix} \cos(\theta+\phi-90°) & -\sin(\theta+\phi-90°) \\ \sin(\theta+\phi-90°) & \cos(\theta+\phi-90°) \end{bmatrix} \qquad (9)$$

In (9), $-90°$ is the offset angle between the global and the local frames where $\theta = \phi = 0$.

(7) and (8) can be transformed to velocity on the local frame, as shown in (10), using the rotation matrix described as (9).

$$\begin{aligned}\begin{bmatrix} v_x^{\mathrm{robot}} \\ v_y^{\mathrm{robot}} \end{bmatrix} &= \boldsymbol{R}^{\mathbf{global}^{-1}}_{\mathbf{robot}} \begin{bmatrix} \dot{x} \\ \dot{y} \end{bmatrix} \\ &= \begin{bmatrix} l_2 - R\cos\theta & l_2 \\ -l_1 + R\cos\theta & -l_1 \end{bmatrix} \begin{bmatrix} \dot{\phi} \\ \dot{\theta} \end{bmatrix} \qquad (10)\end{aligned}$$

By solving (10) for $\dot{\phi}$ and $\dot{\theta}$, (3) is obtained.

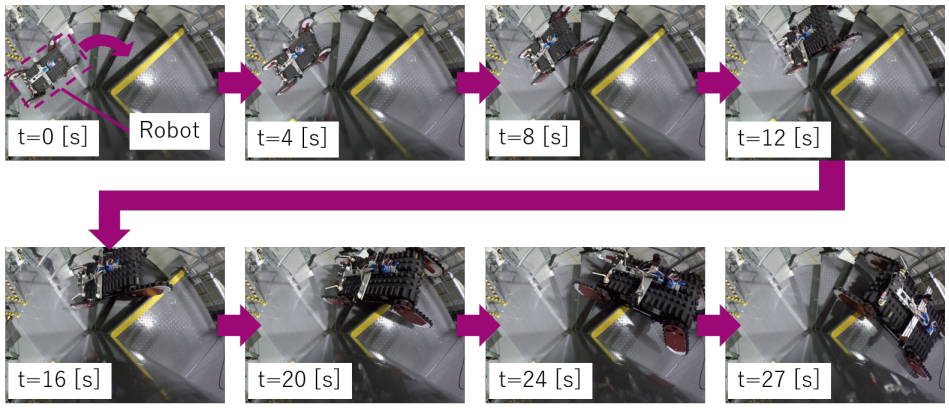

Fig. 14. Snapshot of spiral stair climbing. The robot successfully climbed up the stairs for all seven trials.

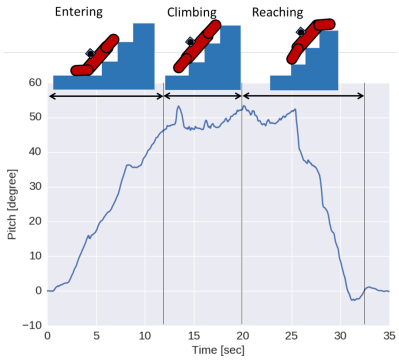

Fig. 15. Time series data of pitch inclination during autonomous spiral stair climbing. The maximum inclination is 53°.

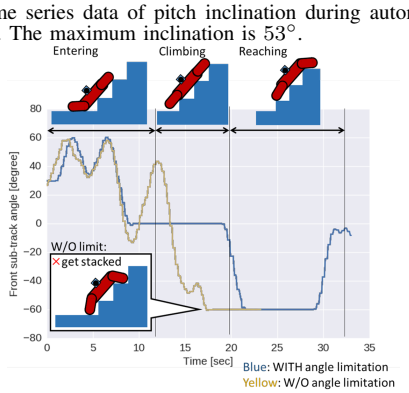

Fig. 16. Time series data of angle of front-right sub-track during autonomous spiral stair climbing. The blue line shows the results of our proposed method. The sub-track was raised when the robot entered the stairs, remained flat during climbing, and lowered when it arrived at the upper floor. This result shows that the strategy in Fig.3 was realized. For a comparison, the yellow line shows the result of the WITHOUT sub-track angle limitation originally introduced herein. In this case, the robot was stacked on the stairs in all trials because the sub-tracks were lowered on the stairs.

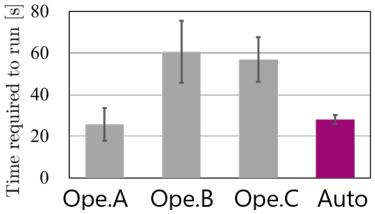

Fig. 17. Operation time of spiral stair climbing. The operation time is compared with three human operators. The results show that the operation time is faster in proposed method compared with operator B and C, and it is slightly slower than operator A.

ACKNOWLEDGMENT

This research has been partially supported by CREST Recognition, Summarization and Retrieval of Large-Scale Multimedia Data.

REFERENCES

[1] Y. Ohashi, S. Kojima, K. Ohno, Y. Okada, R. Hamada, T. Suzuki, and S. Tadokoro, "Attempt at climbing of spiral staircase for tracked vehicles using reaction force of stairs' handrail," in *2017 IEEE/SICE International Symposium on System Integration (SII)*, pp. 456–462, 2017.

[2] J. Liu, Y. Wang, S. Ma, and B. Li, "Analysis of stairs-climbing ability for a tracked reconfigurable modular robot," in *2005 IEEE International Safety, Security and Rescue Robotics (SSRR), Workshop*, pp. 36–41, 2005.

[3] C. Tseng, I. Li, Y. Chien, M. Chen, and W. Wang, "Autonomous stair detection and climbing systems for a tracked robot," in *2013 International Conference on System Science and Engineering (ICSSE)*, pp. 201–204, IEEE, 2013.

[4] J. A. Hesch, G. L. Mariottini, and S. I. Roumeliotis, "Descending-stair detection, approach, and traversal with an autonomous tracked vehicle," in *2010 IEEE/RSJ International Conference on Intelligent Robots and Systems (IROS)*, pp. 5525–5531, IEEE, 2010.

[5] D. Endo and K. Nagatani, "Assessment of a tracked vehicle's ability to traverse stairs," *ROBOMECH Journal*, vol. 3, no. 1, p. 20, 2016.

[6] K. Ohno, S. Morimura, S. Tadokoro, E. Koyanagi, and T. Yoshida, "Semi-autonomous control system of rescue crawler robot having flippers for getting over unknown-steps," in *2007 IEEE/RSJ International Conference on Intelligent Robots and Systems*, pp. 3012–3018, 2007.

[7] Y. Okada, K. Nagatani, and K. Yoshida, "Semi-autonomous operation of tracked vehicles on rough terrain using autonomous control of active flippers," in *2009 IEEE/RSJ International Conference on Intelligent Robots and Systems (IROS)*, pp. 2815–2820, 2009.

[8] F. Colas, S. Mahesh, F. Pomerleau, M. Liu, and R. Siegwart, "3d path planning and execution for search and rescue ground robots," in *2013 IEEE/RSJ International Conference on Intelligent Robots and Systems*, pp. 722–727, 2013.

[9] Y. Ohashi, S. Kojima, K. Ohno, Y. Okada, R. Hamada, T. Suzuki, and S. Tadokoro, "Generation of turning motion for tracked vehicles using reaction force of stairs' handrail," in *11th Conference on Field and Service Robotics (FSR)*, Springer, 2017.

[10] K. Koyanagi, H. Hirukawa, S. Hattori, M. Morisawa, S. Nakaoka, K. Harada, and S. Kajita, "A pattern generator of humanoid robots walking on a rough terrain using a handrail," in *2008 IEEE/RSJ International Conference on Intelligent Robots and Systems (IROS)*, pp. 2617–2622, IEEE, 2008.

[11] M. Kudruss, M. Naveau, O. Stasse, N. Mansard, C. Kirches, P. Soueres, and K. Mombaur, "Optimal control for whole-body motion generation using center-of-mass dynamics for predefined multi-contact configurations," in *2015 IEEE-RAS 15th International Conference on Humanoid Robots (Humanoids)*, pp. 684–689, IEEE, 2015.

[12] O. Khatib and S. Chung, "Suprapeds: Humanoid contact-supported locomotion for 3d unstructured environments," in *2014 IEEE International Conference on Robotics and Automation (ICRA)*, pp. 2319–2325, IEEE, 2014.

[13] D. Kohanbash, S. Moreland, and D. Wettergreen, "Plowing for rover control on extreme slopes," in *Field and Service Robotics*, pp. 399–413, Springer, 2014.